BIOCHEMISTRY
including biophysical chemistry & molecular biology

Article

pubs.acs.org/biochemistry

Crystal Structures of Phosphite Dehydrogenase Provide Insights into Nicotinamide Cofactor Regeneration

Yaozhong Zou,[†] Houjin Zhang,[†] Joseph S. Brunzelle,[⊥] Tyler W. Johannes,[‡] Ryan Woodyer,[§] John E. Hung,[§] Nikhil Nair,[‡] Wilfred A. van der Donk,[†,§] Huimin Zhao,[†,‡,§,∥] and Satish K. Nair*[,†,∥]

[†]Department of Biochemistry, [‡]Department of Chemical and Biomolecular Engineering, [§]Department of Chemistry, and [∥]Center for Biophysics and Computational Biology, University of Illinois at Urbana-Champaign, 600 South Mathews Avenue, Urbana, Illinois 61801, United States

[⊥]Life Sciences Collaborative Access Team, Argonne National Laboratories, Argonne, Illinois 60439, United States

ABSTRACT: The enzyme phosphite dehydrogenase (PTDH) catalyzes the NAD$^+$-dependent conversion of phosphite to phosphate and represents the first biological catalyst that has been shown to conduct the enzymatic oxidation of phosphorus. Despite investigation for more than a decade into both the mechanism of its unusual reaction and its utility in cofactor regeneration, there has been a lack of any structural data for PTDH. Here we present the cocrystal structure of an engineered thermostable variant of PTDH bound to NAD$^+$ (1.7 Å resolution), as well as four other cocrystal structures of thermostable PTDH and its variants with different ligands (all between 1.85 and 2.3 Å resolution). These structures provide a molecular framework for understanding prior mutational analysis and point to additional residues, located in the active site, that may contribute to the enzymatic activity of this highly unusual catalyst.

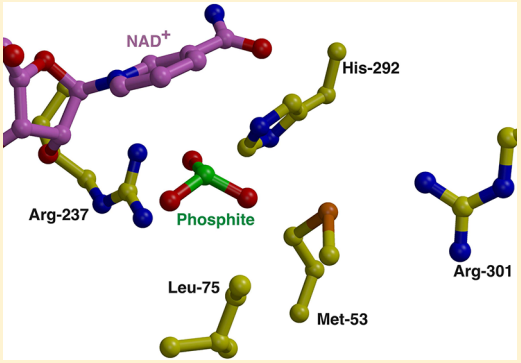

In spite of the fact that a number of bacteria have been shown to conduct oxidation or reduction of phosphorus compounds,[1] enzyme-mediated redox chemistry of phosphorus remains poorly characterized. Enzymatic catalysis of phosphorus redox chemistry has been reported in the NAD$^+$-dependent phosphite oxidoreductase from *Pseudomonas fluorescens* 195,[2,3] and in the hypophosphite oxidase from *Bacillus caldolyticus*.[4] More recently, selection of strains capable of surviving on hypophosphite or phosphite as the sole phosphorus source led to the identification of *Pseudomonas stutzeri* WM88 as an efficient oxidizer of reduced phosphorus compounds.[5] Genetic characterization of this strain demonstrated that the oxidation of hypophosphite to phosphate occurs in two distinct steps, and the gene clusters responsible for these steps have been identified.[6] The *htx* locus encodes a 2-oxoglutarate-dependent dioxygenase that catalyzes the oxidation of hypophosphite to phosphite.[7] The *ptx* locus encodes a gene product PtxD (PTDH, phosphite dehydrogenase) that catalyzes the NAD$^+$-dependent oxidation of phosphite (Scheme 1).[8] Homogeneous preparations of recombinant PDTH were shown to catalyze the oxidation of phosphite to phosphate, coupled with the reduction of NAD$^+$ to NADH, the first characterization of enzymatic oxidation of phosphorus.

Scheme 1. Overall Reaction Catalyzed by PTDH

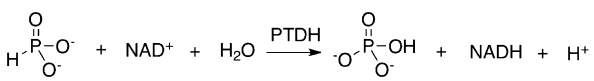

Sequence comparisons place PTDH within the family of NAD$^+$-dependent D-2-hydroxyacid dehydrogenases,[9] and multiple-sequence alignments reveal that PTDH is 26−33% identical with other members of this family. On the basis of the existing structures of D-2-hydroxyacid dehydrogenases[10−14] and by analogy to the reaction mechanism catalyzed by these enzymes, three conserved catalytic residues have been identified as being essential for catalysis by PTDH.[8] A conserved histidine residue (His-292 in PTDH) is proposed to act as a general base in activating the nucleophilic water molecule for attack on phosphite; Glu-266 is believed to both orient and modulate the pK_a of the active site histidine, and Arg-237 is proposed to bind and orient the substrate phosphite prior to nucleophilic attack.[15] Steady state analyses of site-specific variants at each of these residues demonstrate that mutation at His-292 and nonconservative mutations at Arg-237 severely compromise catalysis. Replacement of Glu-266 with Gln results in an unexpected improvement in k_{cat}, but with an overall decreased catalytic efficiency relative to that of the wild type.[16]

Biochemical studies with a number of compounds have failed to identify an alternate substrate for the oxidation reaction,[17] and other members of the D-hydroxyacid dehydrogenase family are incapable of conducting phosphite oxidation. These and other studies lend credence to the biological role of phosphite dehydrogenase as a bona fide phosphite-oxidizing enzyme.[18]

Received: November 10, 2011
Revised: March 22, 2012
Published: May 7, 2012

ACS Publications © 2012 American Chemical Society

The only known effective inhibitor of the enzyme is sulfite (SO_3^{2-}), a competitive inhibitor with phosphite (K_i = 16 μM) thought to act by forming a covalent adduct with NAD that resembles the transition state of the hydride transfer reaction.[16]

Phosphite dehydrogenase has also drawn considerable attention because of its use as a cofactor regeneration system for use during the enzymatic preparation of enantiomerically enriched products.[19] The reduction of NAD^+ to NADH by phosphite dehydrogenase has applications in cofactor recycling in enzymatic processes that utilize NADH or NADPH as a hydride donor.[20−22] The equilibrium constant for the oxidation of phosphite by PTDH can be estimated to be 10^{11}, indicating that the reaction is essentially irreversible.[8] The strong thermodynamic driving force for catalysis and the relatively inexpensive substrate phosphite have made PTDH an attractive candidate for use in the enzymatic regeneration of NADH from NAD^+.[23,24]

Although phosphite dehydrogenase can efficiently utilize NAD^+ to regenerate NADH, the wild-type enzyme is incapable of utilizing $NADP^+$ as a cofactor. To expand the utility of PTDH as a universal nicotinamide cofactor regeneration enzyme, site-specific variants at the active site were generated on the basis of analysis of a homology model structure.[25] Two putative active site residues, Glu-175 and Ala-176, were identified as possible determinants of cofactor specificity. These modeling studies suggested that Glu-175 may interact with the adenine hydroxyl groups of NAD^+ and thus would sterically clash with the 2′-phosphate of $NADP^+$, while replacement of Ala-176 with a basic residue would favorably stabilize the 2′-phosphate of $NADP^+$. Kinetic analyses of the Glu-175 → Ala/Ala-176 → Arg double variant demonstrated a 1000-fold improvement in the catalytic efficiency with $NADP^+$ as a substrate, relative to that of the wild type.[25] This double variant also demonstrated an unexpected 4-fold increase in catalytic efficiency with NAD^+ as a substrate, although the structural foundations for this improvement have not been borne out.

To further aid in the mechanistic elucidations of this biologically unusual catalyst and to provide a molecular basis for further engineering efforts for improved NAD(P)H regeneration, we have elucidated five different crystallographic structures of a thermostable variant of PTDH,[26] as well as those of several active site mutants, bound to various cofactors. This thermostable PTDH variant (hereafter, TS-PTDH to reflect the use of the thermostable variant) was generated by directed evolution and random mutagenesis and contains 16 mutations (see Experimental Procedures for details) that result in increased thermostability and increased activity but with kinetic isotope effects and pre-steady state kinetic parameters similar to those for the wild-type enzyme.[27] The crystal structures presented here consist of the binary complex of TS-PTDH with NAD^+ at 1.7 Å resolution, the TS-PTDH−NAD^+−sulfite ternary complex at 2.2 Å resolution, the relaxed cofactor specificity variant Glu-175 → Ala TS-PTDH−NAD^+ binary complex at 2.3 Å resolution, the cofactor specificity double variant Glu-175 → Ala/Ala-176 → Arg TS-PTDH−NAD^+ binary complex at 1.9 Å resolution, and the Glu-175 → Ala/Ala-176 → Arg TS-PTDH−$NADP^+$ binary complex at 1.85 Å resolution. The crystallographically independent copies observed in crystals of the Glu-175 → Ala TS-PTDH−NAD^+ complex contain both ligand-bound and apo forms of the enzyme. Hence, these five structures provide six distinct chemical views of TS-PTDH representing the "wild type" and variant enzymes interacting with either NAD^+ or $NADP^+$ cofactors, and with the competitive inhibitor sulfite.

EXPERIMENTAL PROCEDURES

Protein Expression and Purification. The expression constructs for the thermostable PTDH, as well as those for the Glu-175 → Ala single and Glu-175 → Ala/Ala-176 → Arg double mutant, have been described previously.[16,25,26] The TS-PTDH variant contains mutations at the following 16 residues, from wt-PTDH from *P. stutzeri*: Asp-13 → Glu, Met-26 → Ile, Val-71 → Ile, Glu-130 → Lys, Gln-132 → Arg, Gln-137 → Arg, Ile-150 → Phe, Gln-215 → Leu, Arg-275 → Gln, Leu-276 → Gln, Ile-313 → Leu, Val-315 → Ala, Ala-319 → Glu, Ala-325 → Val, Glu-332 → Asn, and Cys-336 → Asp. The expression vectors were introduced into *Escherichia coli* BL21(DE3) competent cells, subject to antibiotic selection (ampicillin at a concentration of 100 μg/mL), and individual colonies were grown in 10 mL of LB medium supplemented with ampicillin (100 mg/mL) at 37 °C overnight. Each culture was transferred to fresh LB medium with the same antibiotics and grown until the optical density at 600 nm reached approximately 0.4. The temperature was then decreased to 16 °C; protein production was induced via the addition of 0.4 mM IPTG, and the cells were grown for an additional 18 h. For growth of selenomethionine-labeled TS-PTDH, a 200 μL starter culture was inoculated in minimal medium (6 g/L Na_2HPO_4, 3 g/L KH_2PO_4, 1 g/L NH_4Cl, and 0.5 g/L NaCl) supplemented with 2 mM $MgSO_4$, 0.5% glucose, and 0.05% glycerol and grown at 37 °C overnight. The starter culture (8 mL) was then used to inoculate 800 mL of the same supplemented minimal medium additionally containing adenosine monophosphate (1 μg/mL) and thiamine (1 μg/mL). After growth at 37 °C to an OD_{600} of 1.0, the temperature was reduced to 16 °C, and 5 mL of amino acid mix (lysine, threonine, and phenylalanine at 14 mg/mL each; leucine, isoleucine, and valine at 7 mg/mL each; and 8.4 mg/mL selenomethionine) was added. Twenty minutes later, protein expression was induced with 0.4 mM IPTG, and the cells were grown for an additional 18 h.

Cells were harvested by centrifugation (5000 rpm at 4 °C for 15 min) and resuspended in 50 mL of lysis buffer [50 mM Tris-HCl (pH 7.5) and 300 mM KCl] supplemented with a cocktail of protease inhibitors (2 mM 2-aminoethylbenzenesulfonyl fluoride, 0.3 μM aprotinin, 130 μM bestatin, and 1 μM leupeptin). Cells were disrupted using an Emulsiflex C5 French press cell (Avestin Inc., Ottawa, ON), and the lysate was clarified by centrifugation (15000 rpm at 4 °C for 30 min). The supernatant was filtered through a 0.22 μm pore size Durapore membrane (Millipore, Bedford, MA). The filtrate was applied to HisTrap FF 5 mL (GE Healthcare, Piscataway, NJ) column, and unbound proteins were washed with 20 column volumes of lysis buffer. The bound proteins were eluted with elution buffer [50 mM Tris-HCl (pH 7.5), 300 mM KCl, and 250 mM imidazole] and dialyzed overnight against a solution of 50 mM Tris-HCl (pH 8.5) and 100 mM KCl.

Protein Crystallization. Prior to crystallization, the polyhistidine affinity tag was cleaved using thrombin and the resultant sample was further purified using anion exchange chromatography (5 mL HiTrap Q, GE Healthcare) using a gradient of increasing KCl concentrations and by size-exclusion chromatography (Sephacryl 200, GE Healthcare) in a buffer consisting of 20 mM Na^+-HEPES (pH 7.5) and 100 mM KCl. Protein concentrations were determined using the Bradford method prior to crystallization. Initial crystallization conditions

Table 1. Data Collection, Phasing, and Refinement Statistics

	PTDH−NAD$^+$	PTDH−NAD$^+$−sulfite	SeMet-labeled Glu-175 → Ala PTDH−NAD$^+$	Glu-175 → Ala/Ala-176 → Arg PTDH−NAD$^+$	Glu-175 → Ala/Ala-176 → Arg PTDH−NADP$^+$
			Data Collection[a]		
PDB entry	4E5N	4E5K	4EBF	4E5P	4E5M
space group	$P2_1$	$P2_1$	$P2_1$	$P2_1$	$P2_1$
a, b, c (Å)	90.7, 113.5, 130.2	73.1, 114.2, 88.3	70.2, 122.6, 135.0	70.3, 122.3, 134.3	48.2, 114.0, 58.8
β (deg)	100.2	112.3	96.4	96.4	94.1
resolution (Å)	80−1.7 (1.8−1.7)	82−1.95 (2.0−1.95)	50−2.3 (2.38−2.3)	50−1.9 (1.97−1.9)	50−1.85 (1.92−1.85)
R_{sym} (%)	5.4 (43.6)	6.8 (41.0)	8.2 (37.3)	7.4 (33.9)	7.1 (18.9)
$I/\sigma(I)$	19.2 (3.0)	16.27 (3.2)	19.4 (3.9)	17.8 (3.5)	19.8 (5.3)
completeness (%)	95.0 (74.1)	97.8 (84.9)	98.9 (98.3)	97.6 (89.6)	96.6 (79.3)
redundancy	6.0 (3.8)	4.6 (3.5)	4.1 (4.1)	4.2 (3.9)	4.3 (3.0)
			Refinement		
resolution (Å)	25.0−1.7	25.0−1.95	25.0−2.3	25.0−1.9	25.0−1.85
no. of reflections	256745	90507	91875	163207	49262
R_{work}/R_{free}[b]	21.0/24.7	21.9/26.5	20.8/27.5	20.3/24.3	18.7/21.9
no. of atoms					
protein	20133	10066	15030	15076	5035
NAD$^+$/NADP$^+$	352	176	176	264	96
sulfite	–	16	–	–	–
water	2458	570	754	1338	516
B factor (Å^2)					
protein	29.0	11.5	40.2	29.5	14.9
NAD$^+$/NADP$^+$	23.7	26.1	40.6	33.6	21.8
sulfite	–	33.4	–	–	–
water	38.3	14.3	38.6	36.4	24.3
rmsd					
bond lengths (Å)	0.007	0.013	0.012	0.009	0.007
bond angles (deg)	1.16	1.55	1.55	1.29	1.14

[a]Data for the highest-resolution shell are given in parentheses. [b]$R = \sum(|F_{obs}| - k|F_{calc}|)/\sum|F_{obs}|$, and R_{free} is the R value for a test set of reflections consisting of a random 5% of the diffraction data not used in refinement.

were established with commercial screens from Hampton Research (Aliso Viejo, CA) and Emerald Biosystems (Bainbridge Island, WA). Refinement of promising conditions yielded large crystals suitable for diffraction analysis. Typically, 2 μL of variant TS-PTDH at 10 mg/mL [in 100 mM KCl and 10 mM Na$^+$-HEPES (pH 7.5)] was added to 2 μL of precipitant (0.2 M KCl and 25−30% polyethylene glycol 3350) using buffers with a pH range of 6.5−8.0 (typically 50 mM Na$^+$-MES monohydrate at pH 6.5, 50 mM Na$^+$-HEPES at pH 7.5, or 50 mM Tris-HCl at pH 8.0) and equilibrated over a well containing the precipitant solution at 8 °C. For cocrystallization experiments, the appropriate ligand was added to the protein sample at a final concentration of 5 mM and kept on ice for 30 min prior to crystallization. Crystals grew over a period of 3 weeks and, after transient immersion into a precipitant solution supplemented with 25% glycerol, were vitrified by direct immersion in liquid nitrogen.

Determination and Refinement of the Structure. Crystallographic phases were determined by single-wavelength anomalous diffraction using crystals of selenomethionine (SeMet)-labeled Glu-175 → Ala TS-PDTH, as crystals of this variant could be grown reproducibly. Using crystals of SeMet-labeled Glu-175 → Ala TS-PDTH, a 4-fold redundant anomalous diffraction data set was collected to 2.3 Å resolution using a Mar 300 CCD detector, at an insertion device synchrotron beamline (LS-CAT Sector 21 ID-D, Advanced Photon Source, Argonne, IL), and integrated and scaled using the HKL2000 package.[28] Initial heavy atom positions were determined using HySS (36 SeMet sites) and subjected to maximum likelihood refinement using SHARP (figure of merit = 0.313).[29] The resultant map was of excellent quality and allowed for independent manual modeling of all six copies of the polypeptide in the crystallographic asymmetric unit using XtalView.[30] Despite incubation with a stoichiometric excess of NAD$^+$ prior to crystallization, only four of the molecules in the asymmetric unit exhibit density corresponding to a well-bound nucleotide molecule. As a result, there are considerable differences in the relative orientations of the two domains among the six independent molecules in the asymmetric unit. Noncrystallographic symmetry restraints were not used at any point during refinement. The final model was further improved by crystallographic refinement using REFMAC5, interspersed with rounds of manual model building.[31,32]

The structures of all other variants of TS-PDTH and respective ligand complexes were determined by molecular replacement using the final refined coordinates of one monomer of Glu-175 → Ala TS-PDTH as a search probe. Successful molecular replacement solutions could be determined only by conducting independent searches using the two individual domains of the molecule. After rigid body refinement of the initial molecular replacement solution, the atomic model was subject to automatic rebuilding using ARP/wARP,[33] resulting in nearly complete traces of each of the structures. Cycles of manual rebuilding followed by crystallographic

dx.doi.org/10.1021/bi2016926 | Biochemistry 2012, 51, 4263−4270

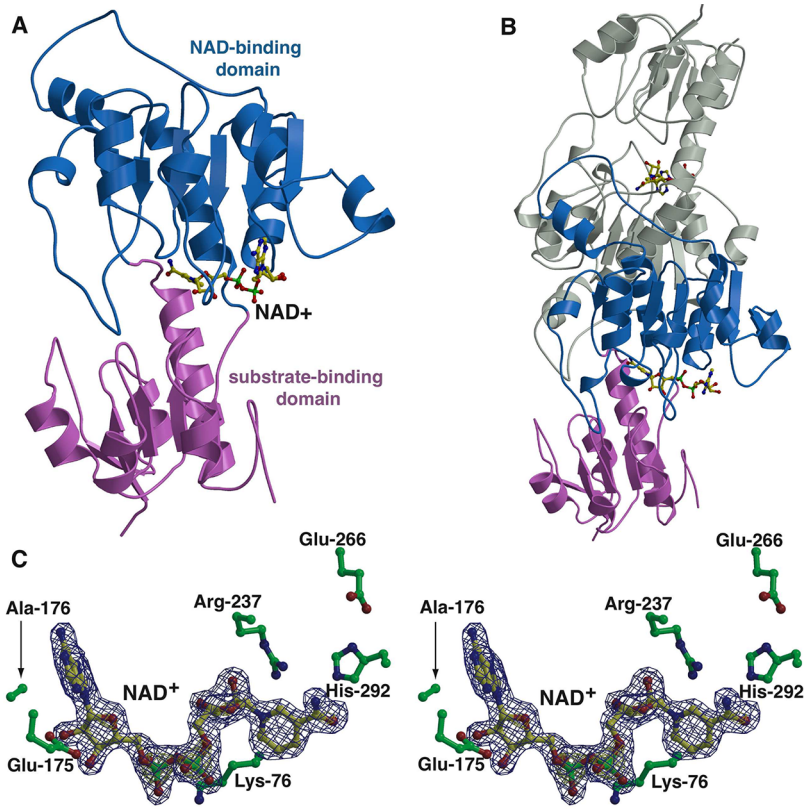

Figure 1. Overall structure of PTDH. (A) Ribbon diagram derived from the 1.75 Å resolution crystal structure of the thermostable PTDH variant showing the disposition of the substrate binding domain (pink) and the NAD binding domain (blue). The bound NAD^+ cofactor is shown as yellow balls and sticks. (B) Structure of the TS-PTDH homodimer with one monomer in the same orientation and color scheme as in panel A and the other monomer colored gray. (C) Close-up view of the NAD^+ binding site. The cofactor is shown as yellow balls and sticks, and active site residues are colored green. Superimposed is a difference Fourier electron density map contoured at the 3σ level over background (blue) and the 8σ level over background (yellow), calculated with $|F_{obs}| - |F_{calc}|$ coefficients and phases from the final refined model with the coordinates of NAD^+ deleted prior to one round of refinement.

refinement were conducted for each of the cocrystal structures. The respective ligands were manually built into the difference Fourier maps after R_{free} values dropped below 30%. Cross-validation, using 5% of the data for the calculation of R_{free}, was utilized throughout the model building process to monitor building bias.[34] The stereochemistry of the models was routinely monitored throughout the course of refinement using PROCHECK.[35] The refined coordinates have been deposited in the Protein Data Bank (PDB).

RESULTS AND DISCUSSION

Determination of the Structure. The crystal structure of the thermostable variant of PTDH, with an additional relaxed cofactor specificity mutation Glu-175 → Ala, in complex with NAD^+, was determined to a resolution of 2.3 Å by single-wavelength anomalous diffraction. The structures of all other active site variants and ligand complexes were determined by molecular replacement. Crystal parameters, data collection parameters, and refinement statistics for each of the structures are summarized in Table 1.

Overall Structure. Our structural studies utilized a thermostable variant of PDTH, and the 1.7 Å resolution cocrystal structure of this variant will be described as the wild-type structure. As expected from the low, but significant, degree of similarity in primary sequence to members of the D-2-hydroxyacid dehydrogenases family, the core architecture of TS-PTDH is similar to those of other enzymes within this group (Figure 1A). Notable structural homologues include *Pyrococcus horikoshii* glyoxylate reductase (PDB entry 2DBQ, *Z* score = 41, rmsd of 1.6 Å over 319 aligned Cα atoms, 34% identical sequence), *Hyphomicrobium methylovorum* glycerate dehydrogenase (PDB entry 1GDH, *Z* score = 35.6, rmsd of 2.4 Å over 317 aligned Cα atoms, 29% identical sequence), and *Aquifex aeolicus* lactate dehydrogenase (PDB entry 3KB6, *Z* score = 34.5, rmsd of 2.2 Å over 312 aligned Cα atoms, 25% identical sequence). Similar to other members of the D-2-hydroxyacid dehydrogenase superfamily, TS-PTDH exists both in solution and in the crystal as a dimer. The multiple copies in the crystallographic asymmetric unit for the various complexes pack as sets of equivalent homodimers.

The TS-PTDH monomer may be divided into a large and a small domain, separated by a flexible hinge region. The large domain (NAD^+ binding domain) is composed of a contiguous stretch of residues from Leu-100 to Pro-291 and consists of six parallel β-strands, sandwiched between seven α-helices. The small domain (substrate binding domain) consists of secondary structural elements from two noncontiguous regions of the polypeptide: Met-1−Val-96 form a domain containing five parallel β-strands flanked by four α-helices, and the segment of Ala-299−Pro-329 contains an additional helix (Figure 1A,B).

The NAD^+ cofactor is housed at the junction between the two domains, where residues from the large subunit engage in interactions with the ligand (Figure 1C). The adenine ring is nestled between two loops composed of His-174−Ala-178 and

dx.doi.org/10.1021/bi2016926 | *Biochemistry* 2012, 51, 4263−4270

Ala-207−Thr-214 and makes van der Waals contacts with Leu-151, Ala-176, and Leu-208. Lys-76 engages in favorable electrostatic interactions with the diphosphate oxygens of the cofactor. The only other consequential interaction with the cofactor occurs through the interaction of Glu-175 with the 2′- and 3′-hydroxyls of the adenine ribose (Oε1−2′-OH distance of 2.6 Å and Oε2−3′-OH distance of 2.5 Å). There is a constellation of polar residues near the nicotinamide, in the vicinity of the putative substrate binding region, and these include the canonical His/Glu/Arg triad (Arg-237, Glu-266, and His-292 in PTDH) found in all D-2-hydroxyacid dehydrogenases. The proximity of these residues to the active site had been previously predicted by homology modeling studies, and their importance has been established via mutational analyses.[16,25]

As noted, the use of a thermostable variant of PTDH, which proved amenable to crystallization, is justified by the fact that pre-steady state kinetics for this variant are similar to those for the wild-type enzyme.[27] Mapping of the sites of the mutations onto the crystal structure reveals that all of the changes occur at positions that are distal relative to the active site (Figure 2).

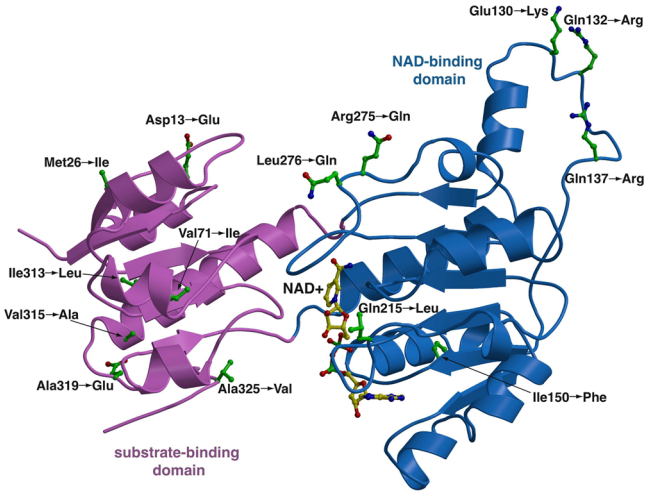

Figure 2. Thermostabilizing mutations in PTDH. Ribbon diagram of the thermostable PTDH variant that was used for structural studies showing the 16 thermostabilizing mutations. Two of the mutations (Glu-332 → Asn and Cys-336 → Asp) occur within the six carboxy-terminal residues that are not visible in the structures. Note that all of these mutations are distal to the active site.

The crystal structure of the TS-PTDH−NAD$^+$ complex also identifies a number of additional polar residues in the vicinity of the active site that may play a role in catalysis. Notable among these is Asp-79 that interacts with Arg-237 and may serve to orient the side chain of the latter to position the substrate phosphite for hydride transfer. Prior mutational analysis of Asp-79 demonstrates that alteration of this side chain results in significant compromises in the catalytic efficiency (a ≤2600-fold decrease in k_{cat}/K_m for the Asp-79 → Ala mutant).[27] Another potentially catalytically relevant residue is Arg-301, which has a side chain that is oriented directly toward the putative substrate binding site but is located >5 Å from this site. Kinetic analysis of site-specific variants at this residue is described in the accompanying paper (DOI 10.1021/bi201691w).

Cocrystal Structure with the Competitive Inhibitor Sulfite. To elucidate the determinants for substrate recognition, we determined the 1.95 Å resolution cocrystal structure of TS-PTDH in complex with NAD$^+$ and the competitive inhibitor sulfite (K_i = 16 μM). The cocrystal structure contains four copies of the TS-PDTH monomer in the crystallographic asymmetric unit, allowing for independent views of the enzyme−inhibitor complex. The sulfite anion is situated proximal to the nicotinamide of the cofactor, where it is engaged through interactions with the side chains of Arg-237 (Nη1−O distance of 2.6 Å and Nη2−O distance of 3.0 Å), His-292 (Nε2−O distance of 2.8 Å), and the backbone amides of Lys-76 (2.8 Å) and Gly-77 (2.7 Å) (Figure 3A). In PTDH, Arg-237, Glu-266, and His-292 constitute the canonical His/Glu/Arg triad found in all D-2-hydroxyacid dehydrogenases, and Asp-79 is proposed to orient the side chain of Arg-237. Our TS-PTDH−sulfite cocrystal structure suggests that these residues are likely involved in positioning the substrate phosphite to facilitate hydride transfer. The cocrystal structure also shows that Arg-301 is oriented toward the sulfite but is located >5 Å from the sulfite oxygen atoms. Kinetic analysis of site-specific mutations at this residue (presented in the accompanying paper) demonstrates that it is important for catalysis (DOI 10.1021/bi201691w). Lastly, local movements near the active site upon binding of sulfite include modest movement of the loop encompassing Ala-74−Phe-78, which results in favorable interactions with the backbone amides, and torsional displacement of the side chain of Met-53 (Sγ−O distance of 3.1 Å), which may facilitate movement of the catalytic hydroxide for attack on the phosphorus atom of the substrate phosphite (Figure 3B).

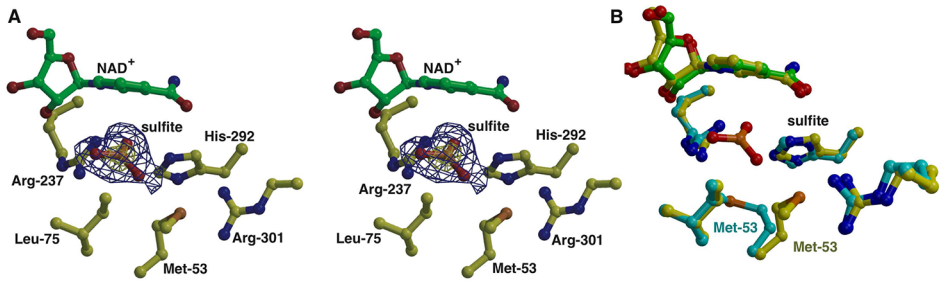

Figure 3. Active site of PTDH in complex with the competitive inhibitor sulfite. (A) The inhibitor is colored orange; the cofactor is shown as green balls and sticks, and active site residues are colored yellow. Superimposed is a difference Fourier electron density map contoured at the 3σ level over background (blue) and the 8σ level over background (yellow), calculated with $|F_{obs}| - |F_{calc}|$ coefficients and phases from the final refined model with the coordinates of sulfite deleted prior to one round of refinement. (B) Superposition of the active sites of unliganded PTDH (cyan) with the sulfite complex (yellow). Note the movement of Met-53 that results in the formation of a defined substrate binding pocket.

dx.doi.org/10.1021/bi2016926 | *Biochemistry* 2012, 51, 4263−4270

Prior spectroscopic analysis suggests that, at the active site, sulfite forms a covalent adduct with NAD^+ that may resemble the transition state for hydride transfer.[17] This adduct was presumed to occur through the covalent linkage of the sulfur to nicotinamide C4. Within the active site of the sulfite cocrystal structure, sulfite is not bound as an adduct but rather as a distinct species. Furthermore, the distance between the sulfur and nicotinamide C4 is 3.9 Å, which is not indicative of a covalently linked adduct. It is currently unclear why an adduct cannot be visualized in the cocrystal structure or even whether the spectroscopic data are truly indicative of an adduct. However, given the long distance of 3.9 Å between the sulfur and nicotinamide C4, modest movements of the enzyme or the substrate and/or cofactor must occur for achievement of a transition state configuration that would optimally place (donor−acceptor distance of 2.7−3.1 Å) the hydrogen of the substrate phosphite over the *re* face of the nicotinamide. Structural studies, molecular dynamics, and cross-correlation analysis are consistent with an ∼0.5 Å movement of the hydride donor to nicotinamide C4 in near-attack ground state conformers of related enzymes of the D-2-hydroxyacid dehydrogenase superfamily.[36]

Crystal Structures of Relaxed Cofactor Specificity Mutants. Attempts to expand the utility of PTDH as a universal nicotinamide cofactor regeneration enzyme capable of also utilizing $NADP^+$ have identified two residues, Glu-175 and Ala-176, as determinants of cofactor specificity.[16] In the wild-type structure, Glu-175 engages both the 2′- and 3′-hydroxyls of the NAD^+ adenine ribose, and this residue would result in steric and electrostatic preclusion of the 2′-phosphate of $NADP^+$ (Figure 1C). Intriguingly, although the Glu-175 → Ala mutant increased $k_{cat}/K_{M,NADP^+}$ (which may approximate the ability of the enzyme to bind the cofactor) by a factor of ∼30, relative to that of the wild type, this variant also demonstrated an unexpected 4-fold increase in $k_{cat}/K_{M,NAD^+}$, despite the anticipated loss of the favorable hydrogen bonds provided by Glu-175.[25] The 2.3 Å resolution cocrystal structure of Glu-175 → Ala TS-PTDH in complex with NAD^+ provides a rationale for the observed increase in $k_{cat}/K_{M,NAD^+}$. Although the overall cocrystal structures of TS and Glu-175 → Ala TS-PTDH with NAD^+ are nearly identical, the Glu-175 → Ala mutation results in local compensatory changes near the vicinity of the bound cofactor (Figure 4A). First, the loop containing residues His-174−Leu-179 moves inward toward the adenine ring of NAD^+, resulting in more favorable van der Waals contact. Second, the movement of this loop results in an orientation of the backbone amide of Ala-175 within hydrogen bonding distance of N3 of adenine (NH−N3 distance of 3.1 Å in the Glu-175 → Ala mutant and 3.6 Å in wild-type TS-PTDH). Finally, the side chain of Leu-208, located on the other side of the adenine ring, also is reoriented, which provides more favorable van der Waals contact with the cofactor. Although these changes are local and are the result of small movements in the variant polypeptide, identical changes can be observed in the multiple, independent copies of Glu-175 → Ala TS-PTDH that are in the crystallographic asymmetric unit. The net result of these movements appears to be better interaction with the NAD^+ cofactor, providing an explanation for the improved $k_{cat}/K_{M,NAD^+}$.

Cofactor specificity has been shown to be further expanded toward $NADP^+$ in the Glu-175 → Ala/Ala-176 → Arg double variant, which increases the $k_{cat}/K_{M,NADP^+}$ by 1000-fold relative to that of the wild type. The 1.9 Å resolution cocrystal structure of Glu-175 → Ala/Ala-176 → Arg TS-PTDH in complex with NAD^+ also demonstrates the compensatory movement of the loop of His-174−Leu-179, relative to that of the wild type, observed in the single mutant (Figure 4B). The Arg-176 side chain points away from the active site, toward the bulk solvent, and is positioned parallel to the adenine ring of NAD^+. As no additional contacts occur between Arg-176 and NAD^+, this structure explains why $k_{cat}/K_{M,NAD^+}$ is not significantly lowered in this double variant (11.8 μM^{-1} min^{-1}), in comparison with that of the Glu-175 → Ala single mutant (13.1 μM^{-1} min^{-1}).

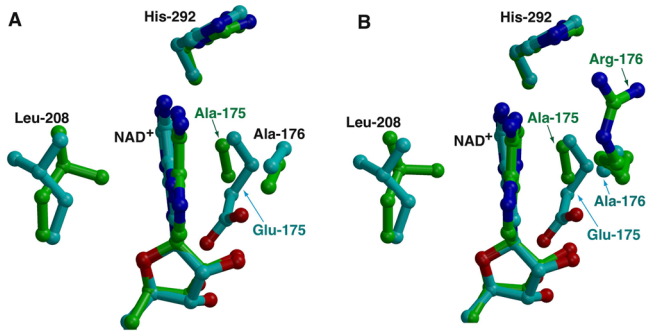

Figure 4. Structures of PTDH variants with relaxed cofactor specificity. (A) Superposition of the structures of complexes of NAD^+ with TS-PTDH (green) and with the Glu-175 → Ala variant (cyan). Note the movements of Ala-175, Ala-176, and Leu-208 toward the adenine ring of the NAD^+ cofactor. (B) Superposition structures of the complexes of NAD^+ with TS-PTDH (green) and with the Glu-175 → Ala/Ala-176 → Arg double variant that can also utilize NADPH as a cofactor (cyan).

To understand the basis for the expanded preference observed only toward $NADP^+$ in this double variant, we determined the 1.85 Å resolution structure of Glu-175 → Ala/Ala-176 → Arg TS-PTDH in complex with $NADP^+$ (Figure 5A). A comparison of the cocrystal structures of the double variants in complex with the two different cofactors reveals that the side chain of Arg-176 rotates away from solvent and faces inward toward the $NADP^+$ phosphate (Figure 5B). Although only one of the phosphate oxygen atoms is within hydrogen bonding distance (Nη2− O distance of 2.6 Å), the other oxygen atoms are within 4 Å of Nε of Arg-176 and are also stabilized by several ordered solvent molecules. The planar stacking of the guanidinium group with the adenine ring of the cofactor further stabilizes the movement of the Arg-176 side chain toward the $NADP^+$ phosphate. Such arginine−aromatic stacking interactions have been previously observed in the structures of the periplasmic ribose binding protein, and P2 myelin, and in *Tritrichomonas foetus* IMP dehydrogenase[37,38] and are suggested to orient the Arg side chain without interfering with the ability to form hydrogen bonds.[39]

Cofactor-Induced Conformational Movement. In the Glu-175 → Ala TS-PDTH structure, only three of the molecules in the asymmetric unit exhibit density corresponding to a well-bound nucleotide molecule, despite incubation of the protein with a 20-fold stoichiometric excess of NAD^+ prior to crystallization. Weak but convincing density, corresponding to a poorly occupied ligand, can be observed in two of the remaining molecules, while the final molecule does not contain any ligand. Consequently, a comparison of the six independent molecules in the crystallographic asymmetric unit of Glu-175 → Ala TS-PDTH allows visualization of the enzyme in conformations with and without a bound cofactor.

dx.doi.org/10.1021/bi2016926 | *Biochemistry* 2012, 51, 4263−4270

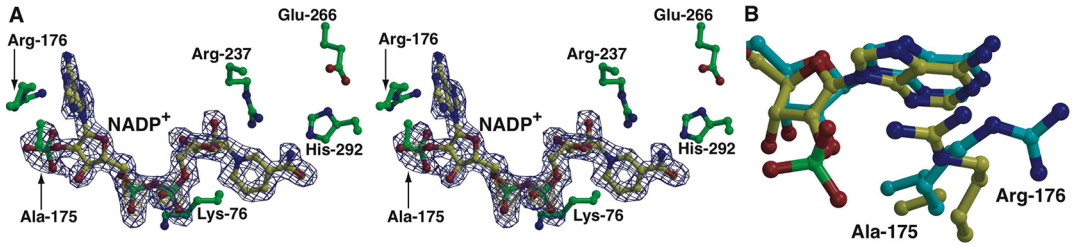

Figure 5. Structure of the relaxed cofactor specificity variant with $NADP^+$. (A) Close-up of the active site of Glu-175 → Ala/Ala-176 → Arg TS-PTDH with bound $NADP^+$. The cofactor is shown as yellow balls and sticks, and active site residues are colored green. Superimposed is a difference Fourier electron density map contoured at the 3σ level over background (blue) and the 8σ level over background (yellow), calculated with $|F_{obs}| - |F_{calc}|$ coefficients and phases from the final refined model with the coordinates of $NADP^+$ deleted prior to one round of refinement. (B) Superposition of the structure of Glu-175 → Ala/Ala-176 → Arg TS-PTDH with bound NAD^+ (cyan) and with bound $NADP^+$ (yellow). Note the movements of Arg-176 toward the phosphate in the $NADP^+$-bound structure.

A comparison of ligand free Glu-175 → Ala TS-PDTH with that of its NAD^+ complex reveals the rigid body rotation characteristic of the family of NAD^+-dependent dehydrogenases.[40] Binding of the cofactor causes the movement of the smaller substrate binding domain toward the larger domain, resulting in a narrowing of the active site cleft. The rigid body movement corresponds to a rotation of ~6° around the hinge region that separates the two domains. As with other enzymes in this same superfamily, the ligand-free conformation can be considered as the "open" conformation and the NAD^+-bound form as the "closed" conformation. In addition to a narrowing of the active site cleft, the transition from the open to the closed conformation results in placement of Lys-76 in a position where it can favorably interact with the diphosphates of NAD^+. In addition, the side chains of Met-53, Leu-75, and Leu-100 close off the active site to shield the bound cofactor from solvent.

CONCLUSION

Phosphite dehydrogenase has drawn considerable attention because of both its role as a catalyst in a biologically unusual reaction and its use in cofactor recycling in bioprocesses that utilize NADH or NADPH as a hydride donor. The cocrystal structures of the thermostable variant of PTDH and various complexes of active site mutants presented here provide a three-dimensional framework for further engineering efforts aimed at improving the catalytic efficiency and expanding the cofactor repertoire. These cocrystal structures also identify a number of active site residues that may function in catalysis, and an additional structure-based functional study aimed at validating the functions of these residues is presented in the accompanying paper (DOI 10.1021/bi201691w).

AUTHOR INFORMATION

Corresponding Author

*Department of Biochemistry, University of Illinois at Urbana-Champaign, 600 S. Mathews Ave., Urbana, IL 61801. Telephone: (217) 333-2688. Fax: (217) 244-5858. E-mail: snair@uiuc.edu.

Funding

This work was supported in part by the National Science Foundation (NSF 0822536 to W.A.v.d.D.) and the Biotechnology Research and Development Consortium (Project 2-4-121 to H. Zhao).

Notes

The authors declare no competing financial interest.

ACKNOWLEDGMENTS

We thank Keith Brister at LS-CAT (21-ID at APS) for facilitating data collection.

ABBREVIATIONS

PTDH, phosphite dehydrogenase; *ptxD*, phosphite dehydrogenase-encoding gene; NAD^+ and NADH, nicotinamide adenine dinucleotide; rmsd, root-mean-square deviation.

REFERENCES

(1) White, A. K., and Metcalf, W. W. (2007) Microbial metabolism of reduced phosphorus compounds. *Annu. Rev. Microbiol. 61*, 379−400.
(2) Malacinski, G., and Konetzka, W. A. (1966) Bacterial oxidation of orthophosphate. *J. Bacteriol. 91*, 578−582.
(3) Malacinski, G. M., and Konetzka, W. A. (1967) Orthophosphite-nicotinamide adenine dinucleotide oxidoreductase from *Pseudomonas fluorescens*. *J. Bacteriol. 93*, 1906−1910.
(4) Lauwers, A. M., and Heinen, W. (1974) Bio-degradation and utilization of silica and quartz. *Arch. Microbiol. 95*, 67−78.
(5) Metcalf, W. W., and Wolfe, R. S. (1998) Molecular genetic analysis of phosphite and hypophosphite oxidation by *Pseudomonas stutzeri* WM88. *J. Bacteriol. 180*, 5547−5558.
(6) White, A. K., and Metcalf, W. W. (2004) The htx and ptx operons of *Pseudomonas stutzeri* WM88 are new members of the pho regulon. *J. Bacteriol. 186*, 5876−5882.
(7) White, A. K., and Metcalf, W. W. (2002) Isolation and biochemical characterization of hypophosphite/2-oxoglutarate dioxygenase. A novel phosphorus-oxidizing enzyme from *Psuedomonas stutzeri* WM88. *J. Biol. Chem. 277*, 38262−38271.
(8) Costas, A. M., White, A. K., and Metcalf, W. W. (2001) Purification and characterization of a novel phosphorus-oxidizing enzyme from *Pseudomonas stutzeri* WM88. *J. Biol. Chem. 276*, 17429−17436.
(9) Grant, G. A. (1989) A new family of 2-hydroxyacid dehydrogenases. *Biochem. Biophys. Res. Commun. 165*, 1371−1374.
(10) Dengler, U., Niefind, K., Kiess, M., and Schomburg, D. (1997) Crystal structure of a ternary complex of D-2-hydroxyisocaproate dehydrogenase from *Lactobacillus casei*, NAD^+ and 2-oxoisocaproate at 1.9 Å resolution. *J. Mol. Biol. 267*, 640−660.
(11) Goldberg, J. D., Yoshida, T., and Brick, P. (1994) Crystal structure of a NAD-dependent D-glycerate dehydrogenase at 2.4 Å resolution. *J. Mol. Biol. 236*, 1123−1140.
(12) Lamzin, V. S., Aleshin, A. E., Strokopytov, B. V., Yukhnevich, M. G., Popov, V. O., Harutyunyan, E. H., and Wilson, K. S. (1992) Crystal structure of NAD-dependent formate dehydrogenase. *Eur. J. Biochem. 206*, 441−452.
(13) Lamzin, V. S., Dauter, Z., Popov, V. O., Harutyunyan, E. H., and Wilson, K. S. (1994) High resolution structures of holo and apo formate dehydrogenase. *J. Mol. Biol. 236*, 759−785.

(14) Schuller, D. J., Grant, G. A., and Banaszak, L. J. (1995) The allosteric ligand site in the V_{max}-type cooperative enzyme phosphoglycerate dehydrogenase. *Nat. Struct. Biol. 2*, 69−76.
(15) Relyea, H. A., and van der Donk, W. A. (2005) Mechanism and applications of phosphite dehydrogenase. *Bioorg. Chem. 33*, 171−189.
(16) Woodyer, R., Wheatley, J. L., Relyea, H. A., Rimkus, S., and van der Donk, W. A. (2005) Site-directed mutagenesis of active site residues of phosphite dehydrogenase. *Biochemistry 44*, 4765−4774.
(17) Relyea, H. A., Vrtis, J. M., Woodyer, R., Rimkus, S. A., and van der Donk, W. A. (2005) Inhibition and pH dependence of phosphite dehydrogenase. *Biochemistry 44*, 6640−6649.
(18) Vrtis, J. M., White, A. K., Metcalf, W. W., and van der Donk, W. A. (2001) Phosphite dehydrogenase: An unusual phosphoryl transfer reaction. *J. Am. Chem. Soc. 123*, 2672−2673.
(19) Vrtis, J. M., White, A. K., Metcalf, W. W., and van der Donk, W. A. (2002) Phosphite dehydrogenase: A versatile cofactor-regeneration enzyme. *Angew. Chem., Int. Ed. 41*, 3257−3259.
(20) Chenault, H. K., and Whitesides, G. M. (1987) Regeneration of nicotinamide cofactors for use in organic synthesis. *Appl. Biochem. Biotechnol. 14*, 147−197.
(21) van der Donk, W. A., and Zhao, H. (2003) Recent developments in pyridine nucleotide regeneration. *Curr. Opin. Biotechnol. 14*, 421−426.
(22) Zhao, H., and van der Donk, W. A. (2003) Regeneration of cofactors for use in biocatalysis. *Curr. Opin. Biotechnol. 14*, 583−589.
(23) Johannes, T. W., Woodyer, R. D., and Zhao, H. (2007) Efficient regeneration of NADPH using an engineered phosphite dehydrogenase. *Biotechnol. Bioeng. 96*, 18−26.
(24) Woodyer, R., van der Donk, W. A., and Zhao, H. (2006) Optimizing a biocatalyst for improved NAD(P)H regeneration: Directed evolution of phosphite dehydrogenase. *Comb. Chem. High Throughput Screening 9*, 237−245.
(25) Woodyer, R., van der Donk, W. A., and Zhao, H. (2003) Relaxing the nicotinamide cofactor specificity of phosphite dehydrogenase by rational design. *Biochemistry 42*, 11604−11614.
(26) Johannes, T. W., Woodyer, R. D., and Zhao, H. (2005) Directed evolution of a thermostable phosphite dehydrogenase for NAD(P)H regeneration. *Appl. Environ. Microbiol. 71*, 5728−5734.
(27) Fogle, E. J., and van der Donk, W. A. (2007) Pre-steady-state studies of phosphite dehydrogenase demonstrate that hydride transfer is fully rate limiting. *Biochemistry 46*, 13101−13108.
(28) Otwinowski, Z., Borek, D., Majewski, W., and Minor, W. (2003) Multiparametric scaling of diffraction intensities. *Acta Crystallogr. A59*, 228−234.
(29) Bricogne, G., Vonrhein, C., Flensburg, C., Schiltz, M., and Paciorek, W. (2003) Generation, representation and flow of phase information in structure determination: Recent developments in and around SHARP 2.0. *Acta Crystallogr. D59*, 2023−2030.
(30) McRee, D. E. (1999) XtalView/Xfit: A versatile program for manipulating atomic coordinates and electron density. *J. Struct. Biol. 125*, 156−165.
(31) Murshudov, G. N., Vagin, A. A., and Dodson, E. J. (1997) Refinement of macromolecular structures by the maximum-likelihood method. *Acta Crystallogr. D53*, 240−255.
(32) Murshudov, G. N., Vagin, A. A., Lebedev, A., Wilson, K. S., and Dodson, E. J. (1999) Efficient anisotropic refinement of macromolecular structures using FFT. *Acta Crystallogr. D55*, 247−255.
(33) Perrakis, A., Sixma, T. K., Wilson, K. S., and Lamzin, V. S. (1997) wARP: Improvement and extension of crystallographic phases by weighted averaging of multiple-refined dummy atomic models. *Acta Crystallogr. D53*, 448−455.
(34) Kleywegt, G. J., and Brunger, A. T. (1996) Checking your imagination: Applications of the free R value. *Structure 4*, 897−904.
(35) Laskowski, R. A., Rullmannn, J. A., MacArthur, M. W., Kaptein, R., and Thornton, J. M. (1996) AQUA and PROCHECK-NMR: Programs for checking the quality of protein structures solved by NMR. *J. Biomol. NMR 8*, 477−486.
(36) Luo, J., and Bruice, T. C. (2004) Anticorrelated motions as a driving force in enzyme catalysis: The dehydrogenase reaction. *Proc. Natl. Acad. Sci. U.S.A. 101*, 13152−13156.
(37) Gan, L., Petsko, G. A., and Hedstrom, L. (2002) Crystal structure of a ternary complex of *Tritrichomonas foetus* inosine 5′-monophosphate dehydrogenase: NAD^+ orients the active site loop for catalysis. *Biochemistry 41*, 13309−13317.
(38) Prosise, G. L., and Lueke, H. (2003) Crystal structures of *Tritrichomonas foetus* inosine monophosphate dehydrogenase in complex with substrate, cofactor and analogs: A structural basis for the random-in ordered-out kinetic mechanism. *J. Mol. Biol. 326*, 517−527.
(39) Flocco, M. M., and Mowbray, S. L. (1994) Planar stacking interactions of arginine and aromatic side-chains in proteins. *J. Mol. Biol. 235*, 709−717.
(40) Eklund, H., and Branden, C. I. (1987) Crystal Structure, Coenzyme Conformations, and Protein Interactions. In *Pyridine Nucleotide Coenzyme: Chemical, Biochemical and Medical Aspects* (Dolphin, D., Poulson, R., and Avramovic, O., Eds.) pp 51−98, Wiley and Sons, New York.